

Contribution of small-angle X-ray scattering to microstructural investigation of newly developed Mg–rare earth alloys for structural applications

Caroline Antion,^{a,b} Françoise Bley,^{a,*} Patricia Donnadiou,^a Alexis Deschamps,^a Alexander Pisch,^a Jean-Jacques Blandin^c and Catherine Tassin-Arques^a

^aLTPCM (UMR 5614 CNRS-INPG-UJF), BP75, 38340 Saint Martin d'Hères Cedex, France, ^bSYMME, Université de Savoie, BP 806, 74016 Annecy, France, and ^cGPM2 (UMR 5010 CNRS-INPG-UJF), BP46, 38340 Saint Martin d'Hères Cedex, France. Correspondence e-mail: francoise.bley@ltpcm.inpg.fr

New Mg–Y–Gd–Mn alloys, strengthened by a dense fine scale precipitation, have been recently designed for structural applications up to 523 K. The qualitative small-angle X-ray scattering study presented here enlightens the mechanical properties at high temperature of these alloys. Small Guinier–Preston zones have been evidenced in alloys maintained at room temperature after quenching. The metastable phases, studied in parallel using high-resolution transmission electron microscopy and responsible for the good mechanical properties, are difficult to quantify completely owing to their complex microstructure of interconnected globular and faceted precipitates.

© 2007 International Union of Crystallography
Printed in Singapore – all rights reserved

1. Introduction

Magnesium–rare earth alloys are potential candidates for structural applications owing to their low density and their ability to be strengthened by a dense fine scale precipitation (Nie & Muddle, 2000; Anyanwu *et al.*, 2001). Some of these alloys may be used up to 523 K: among those are the commercial alloys WE43 (4 wt% Y, 3.3 wt% RE, 0.5 wt% Zr) or WE54 (5 wt% Y, 3.3 wt% RE, 0.5 wt% Zr) (Nie & Muddle, 1999).

New alloys containing Y and Gd have been recently designed and produced by casting (Antion, 2003): 8 wt% Gd, 3 wt% Y, 1 wt% Mn, (balance Mg) further called 8Gd-3Y and 4 wt% Gd, 5 wt% Y, 1 wt% Mn, (balance Mg) further called 4Gd-5Y (Mn has been added in these alloys to prevent them from corrosion).

The study of ageing treatments for these alloys has evidenced a large hardening potential, related to the precipitation of metastable β'' and β' phases as revealed by transmission electron microscopy (TEM) (Antion *et al.*, 2006). Compression and creep tests performed up to 573 K have shown that these alloys display mechanical properties higher than the commercial alloys up to 523 K. However, above 523 K a drop of mechanical properties is observed for all alloys (Antion *et al.*, 2003; Antion, 2003; Antion *et al.*, 2006). The aim of the present paper is to clarify the hardening mechanisms of these alloys by a detailed microstructural study.

Small-angle X-ray scattering (SAXS) has been used as a complementary tool for the study of hardening precipitation for two main reasons: first SAXS is a very efficient technique to characterize fine scale precipitation like Guinier–Preston (GP) zones which are difficult to observe by TEM. Secondly SAXS allows the study of the evolution of the precipitates (density and scale) continuously during thermal cycles and therefore leads to an understanding of the precipitation kinetics during realistic thermal paths.

In addition, SAXS, providing a statistical measurement of a large number of objects, acts as a natural complement to high-resolution TEM (HRTEM), which gives a direct but local view of the microstructure. To our knowledge up to now, very few SAS measurements

have been made on Mg–rare earth alloys (Adachi *et al.*, 2004; Antion *et al.*, 2003) and the present study is somehow a pioneering work in this class of alloys.

2. Materials and methods

Details of the melting and casting of the two 8Gd-3Y and 4Gd-5Y alloys can be found in Antion (2003). Temperatures of solution treatments, under argon atmosphere, for the different alloys are presented in Table 1 and have been determined from a first set of thermodynamic calculations in appropriate phase diagrams (Antion, 2003). Further ageing treatments have been performed under air: T4 is aged at room temperature, T6 is aged at peak hardening, and T8 is over-aged. Two binary alloys have also been prepared: Mg-5%Gd called 5Gd and Mg-5%Y called 5Y.

2.1. Small-angle X-ray scattering

SAXS measurements have been performed on D2AM-BM02 a French CRG beamline at the ESRF (Simon *et al.*, 1997). The usual SAXS camera under vacuum has been used. The sample-to-detector distance was close to 75 cm for all the measurements, and the beam size on the detector was $\sim 200 \mu\text{m} \times 400 \mu\text{m}$. The setup of optics is such that the beam does not move with energy changes less than 1 keV. The detector was a charge coupled device (CCD) camera with indirect illumination; a 2 x 2 binning gives a pixel size of 100 μm .

Table 1
Heat treatments.

	T4	T6	T8
WE43†	8 h 798 K + quench + R.T.	T4 + 4 h 523 K	
5Gd	8 h 798 K + quench + R.T.		
5Y	8 h 798 K + quench + R.T.		
8Gd-3Y	8 h 798 K + quench + R.T.	T4 + 64 h 473 K	T4 + 1104 h 473 K
4Gd-5Y	8 h 753 K + quench + R.T.	T4 + 128 h 473 K	T4 + 1104 h 473 K

† Purchased from Magnesium Elektron Ltd.

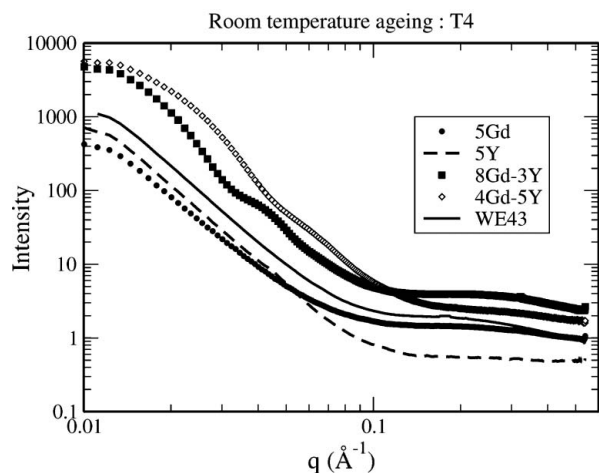


Figure 1
Intensity vs q for all compositions, in the T4 state at 17.03 keV.

After subtraction of the dark field, correction is made for flat field and distortion, and then radial averaging allows for good statistics on the far low-counting regions owing to the high number of pixels (>1000). The main problem of this detector is the fluctuation of the dark current level, which requires an arbitrary constant correction. Samples are polycrystalline with grain size $\simeq 80 \mu\text{m}$, giving a low statistical average. So, when possible, measurements have been performed at nine places in the sample, and averaged. Intensities have been corrected for transmission, thickness and background, and then normalized (relatively) for the different energies using a non-anomalous polyurethane sample.

Measurements have been made at two energy ranges: under the Y edge (17.038 keV) and under the Mn edge (6.539 keV). Sample thicknesses are close to attenuation length, and are different for both edges, close to 600 μm at the Y edge and to 100 μm at the Mn edge.

Energy under the yttrium edge has been chosen for two purposes: (1) to investigate large enough values of the modulus of the scattering vector q [$q = 4\pi\sin(\theta)/\lambda$, 2θ being the scattering angle and λ the wavelength] from 0.01 to 0.5 \AA^{-1} , which allows detection of small particles and (2) to promote contrast variations due to Y precipitation. In particular, varying the energy close to this value should allow

detection of yttrium composition differences between magnesium solid solution and precipitates, whose composition is not clearly established (Antion, 2003; Antion *et al.*, 2003; Antion *et al.*, 2006).

All samples with Y have been measured at six energies (from 8 to 300 eV under Y edge), and samples with no Y only at 17.03 keV. The energy resolution $\Delta E/E$ of the X-ray beam was close to 10^{-4} .

SAXS has been also performed under the Mn absorption edge at 6.24 keV, allowing measurements at lower values of scattering vector q , from 0.004 to 0.18 \AA^{-1} , and so to detect larger particles. Moreover, anomalous measurements of T6 and T8 samples, at six energies (from 9 to 300 eV under Mn edge), have shown negligible contrast variation and then, no implication of Mn in precipitation.

For *in-situ* experiments, a small furnace has been installed to study the evolution of hardening precipitates when further annealing at higher temperatures is carried out on the 8Gd-3Y and 4Gd-5Y alloys after peak ageing (T6 state) and over-ageing (T8 state) as well as on commercial WE43 alloys in T6 state. *In situ* experiments are made at 6.24 keV.

3. Experimental *ex-situ* results

3.1. Initial state T4

Scattering intensities vs q for the two quaternary, the two binary alloys and WE43 in the T4 state, which corresponds to a room temperature ageing of the quenched samples, are presented in Fig. 1. On those curves, there is no subtraction of a constant to correct for 'dark current level' or incoherent scattering. At high q -values, a hump can be observed, close to 0.3 \AA^{-1} , characteristic of GP zones. This hump is more pronounced in the alloy containing the most Gd, and very low in the binary 5Y. In all cases, the sizes of these GP zones are very small, with a gyration radius (Guinier & Fournet, 1955; Porod, 1982) close to 3 \AA , thus including few Y or Gd atoms.

The presence of GP zones was also detected in WE43 alloys in the same T4 state (Antion *et al.*, 2003).

In the two quaternary alloys, the low- q scattering shows oscillations which are enhanced in the Porod plot (Iq^4 vs q) representation [Fig. 2(a)], and are not present in the binary alloy. Such oscillations are characteristic of a narrow distribution of spherical particles, whose average radius has been estimated to 130 \AA in 8Gd-3Y alloys and 90 \AA in 4Gd-5Y alloys; estimations of such contributions are plotted on Fig. 2(a) using a log-normal distribution $\propto \exp\{-[\ln(R/R_m)]^2/2\}$, with σ equal to 0.15 and 0.23, respectively.

Such a precipitation has been evidenced in T4 quaternary alloys owing to TEM observations [Fig. 2(b)]. In both alloys, we observe spherical precipitates which seem to be located in bands near grain boundaries and whose average diameter is close to 200 \AA , in agreement with SAXS estimations. These precipitates have been identified as equilibrium β phase which grows in the temperature range chosen for solution treatment. Indeed, the temperature for solution treatments had been determined from the first calculated Mg-Mn-Y-Gd phase diagram (Antion, 2003), which was corrected afterwards. It appeared that 798 and 753 K temperatures correspond to equilibrium between magnesium solid solution and a small volume fraction of equilibrium β phase, the temperature gap to obtain pure solid solution being very small.

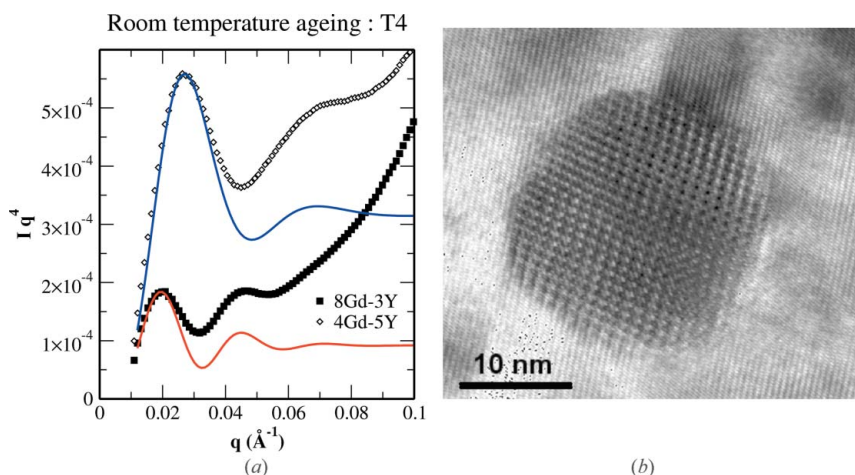


Figure 2
Remaining β equilibrium phase precipitates in quaternary alloys. (a) Porod plot (Iq^4 vs q) in the T4 state at 16.74 keV; estimation of intensities due to log-normal distribution of spheres are shown as continuous lines. (b) HRTEM image of such a precipitate in solution treated (T4) 4Gd-5Y alloy.

Due to the high temperature at which they have appeared, it is not expected that these precipitates will evolve during subsequent heat treatment at low temperature; however, the variability of their contribution from one sample to another will hinder the subtraction of their contribution, which would have been necessary for a full analysis of the metastable precipitation.

Anomalous effect at the Y absorption edge has been measured by varying energy. Neglecting Mn, f_A being the atomic structure factor of element A and $S_{AB}(q)$ the partial structure factor, the intensity, for a ternary alloy (Simon & Lyon, 1987; Goerigk *et al.*, 2003) is written as:

$$I(q) \propto (f_{Gd} - f_{Mg})^2 S_{GdGd}(q) + (f_Y - f_{Mg})^2 S_{YY}(q) + 2(f_{Gd} - f_{Mg})(f_Y - f_{Mg}) S_{GdY}(q). \quad (1)$$

In the simple case of a two-phases model, the partial structure factors are proportional:

$$S_{AB}(q) = \Delta C_A \Delta C_B S_{pm}(q), \quad (2)$$

with ΔC_A the concentration difference of element A between precipitate and matrix.

In this energy range, the contrast values are:

$$(f_{Gd} - f_{Mg})^2 = 2650 \text{ in the whole range} \quad (3)$$

$$(f_Y - f_{Mg})^2 = 550 \text{ at } 16.740 \text{ keV} \quad (4)$$

$$(f_Y - f_{Mg})^2 = 400 \text{ at } 17.030 \text{ keV} \quad (5)$$

In Fig. 3, for the 4Gd-5Y alloy in the T4 state, a small contrast variation can be observed for low values of diffusion vector q , corresponding to β equilibrium precipitates. By integrating intensity between $q = 0.01$ and 0.1 \AA^{-1} , it can be estimated to 25%. For 8Gd-3Y in the T4 state, the observed contrast is only some % and invisible in the binary 5Y. Those results are in agreement with equilibrium properties: the β precipitates have different crystallographic structure for the 2 quaternary alloys, and are Y rich for 4Gd-5Y ($Mg_{24}(Y-Gd)_5$ and Gd rich for 8Gd-3Y $Mg_5(Gd-Y)$). In binary 5Y alloy, the lack of anomalous effect is linked to the absence of any β phase precipitate because of optimized solution treatment of the alloy. This is explained by a larger temperature range for homogenization in binary alloys than in quaternary alloys (Antion, 2003).

In the q region of GP zones it is not easy to have a correct idea about the contrast variation, owing to the required adjustment of background, which was not done in Fig. 3, to illustrate its effect.

3.2. Peak-aged alloys (T6 state)

3.2.1. Mg-Mn-Y-Gd alloys. Apart from volume fraction of precipitates, 8Gd-3Y and 4Gd-5Y alloys present similar precipitation microstructures after peak-ageing treatment at 473 K, like on Fig. 4. The microstructure consists of a fine homogeneous distribution of faceted precipitates formed in prismatic $\{1\bar{1}00\}$ magnesium planes. Average size of precipitates having an approximate globular section is 100 \AA . Such precipitates correspond to the metastable β' phase of the Mg-rare earth precipitation sequence having a bcc crystal structure; the faceted shape of the β' precipitates results from the way in which they are formed: plane by plane from stacking of ordered monoplanar β'' precipitates having a DO_{19} structure every four magnesium planes (Antion, 2003; Antion *et al.*,

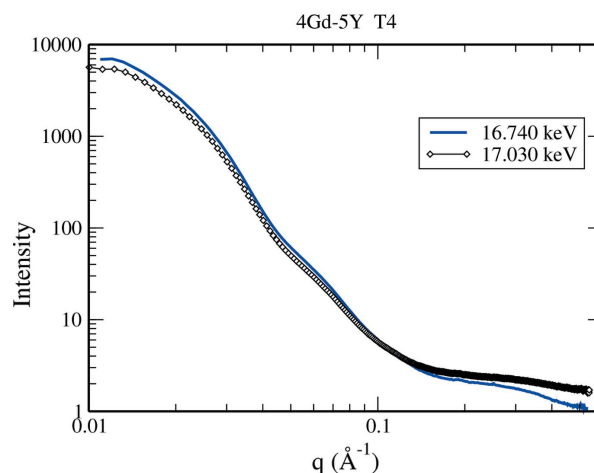


Figure 3 Intensity vs q for the 4Gd-5Y alloy in the T4 state, at two energies under the Y edge, showing anomalous contrast.

2006). The latter corresponds to the formation of the first metastable phase for earlier time of precipitation. Each DO_{19} -ordered plane is well visible on an HRTEM image [Fig. 4(a)]. It is noteworthy that β' precipitates are strongly connected one to another, owing to their type of formation. The resulting microstructure of precipitation presents several characteristic lengths and a rather complicated shape, which makes a full identification of morphological parameters from SAXS images very difficult.

SAXS measurements have been performed at both energy ranges. For both quaternary alloys in the T6 state, two-dimensional SAXS images show streaks [Fig. 4(b)], which we interpret as representative of the plane by plane growth of the bcc β' precipitates, and can be thought as diffraction by the facets. In order to average the streaks, measurements have been made at nine places in the sample, distant by $500 \mu\text{m}$. Those streaks are absent in the T4 states of all alloys and are a signature of the new precipitates.

Precipitates with sharp edges induce a non-oscillating intensity component (Tchoubar & Mering, 1969), which superimpose to that of the still present high-temperature spherical precipitates, evidenced by analogous oscillations of intensity, as can be seen in Fig. 5.

The separation of intensity related to hardening precipitates from that of the β phase is not feasible by subtraction of the T4 intensity from the T6 one, owing to GP zones in the T4 state (that are absent in the T6 state), to contrast modification between matrix and β phase

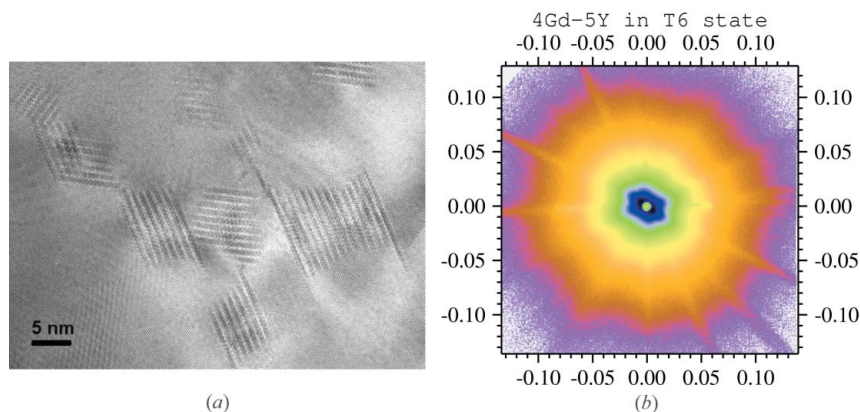


Figure 4 4Gd-5Y alloy after T6 treatment: (a) HRTEM image of faceted β' precipitates; (b) two-dimensional rough intensity map, at one of the positions at 6.24 keV (units on the axes are \AA^{-1} , auto-scaled intensity).

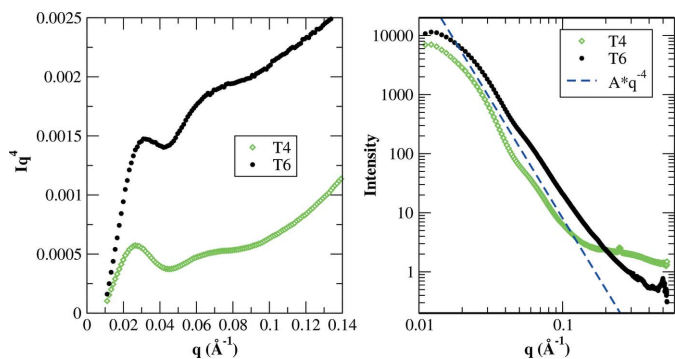


Figure 5 4Gd-5Y (T4 and T6 states) at 16.74 keV: (a) Porod plot (Iq^4 vs q) showing oscillations characteristic of the spherical β particles; a non-oscillating term is superimposed for the T6 state; (b) ln–ln plot of intensity vs q ; the exponent of the asymptotic behaviour is close to four.

induced by unmixing and to some variability in the alloy microstructure preventing to have strictly reproducible intensity from one slice to another.

Analysis of anomalous measurements at the Y edge on the alloys in the T6 state, in the same way as for the T4 state, gives a 10% variation of the contrast for both compositions, indicating a different composition of the β' phase, as compared with the β phase.

3.2.2. WE43 alloy. SAXS measurements have also been performed on industrial WE43 alloys peak-aged at 523 K in the same conditions. In this alloy, the qualitative aspect of intensity is different from that of quaternary alloys. On two-dimensional intensity maps [Fig. 6(b)], streaks are still present but with a different shape. This should be related to the plate-shaped morphology of some β' precipitates in these alloys, as can be seen on the TEM image, Fig. 6(a). Indeed, in WE43 alloys peak-aged at 523 K, β' precipitates have two morphologies: platelets and globular, inherited from two independent types of formation from an earlier ageing state (Antion *et al.*, 2003).

Intensity has also been measured at several places in the sample. Average intensity behaves like q^{-3} , and does not reach the q^{-4} behaviour at large q values, in possible relationship with the mixing of platelets and globular precipitate contributions to intensity (Fig. 7).

3.3. Over-aged quaternary alloys (T8 state)

In over-aged state at 473 K, 8Gd-3Y and 4Gd-5Y alloys still have the same type of precipitation microstructure (Fig. 8). Faceted β'

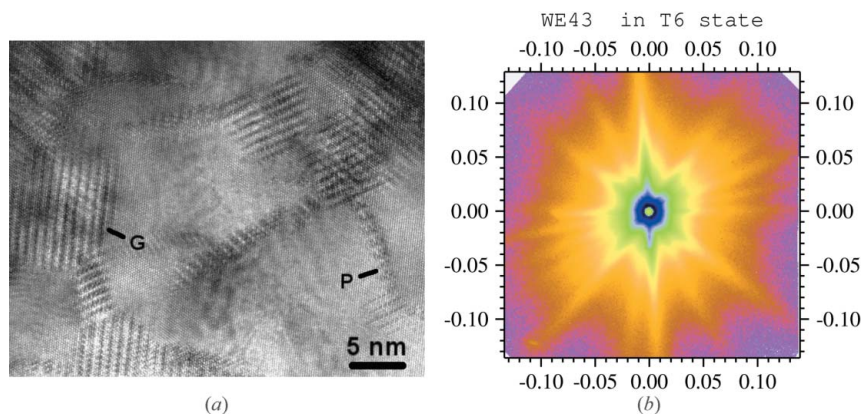


Figure 6 WE43 in the T6 state: (a) high resolution TEM image; P and G show respectively platelets and globular precipitates (b) Two-dimensional rough intensity map, at one of the positions at 6.24 keV (units on the axes are \AA^{-1} , auto-scaled intensity).

Table 2 Evolution of the compression yield stress of quaternary alloys, compared with the industrial WE43, measured at the given temperatures.

T	8Gd-3Y	4Gd-5Y	WE43
473 K	270 MPa	218 MPa	193 MPa
523 K	267 MPa	213 MPa	185 MPa
548 K	211 MPa	140 MPa	160 MPa
573 K	146 MPa	111 MPa	150 MPa

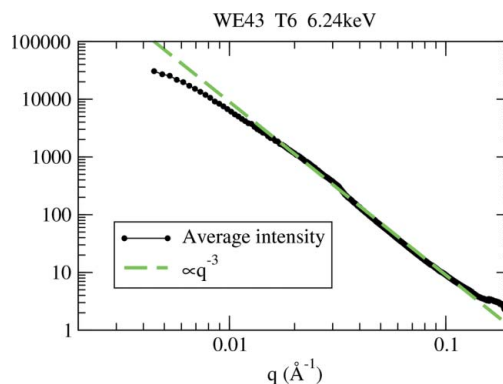


Figure 7 ln–ln plot of intensity averaged for different places in WE43 (T6 state) at 6.24 keV; no background subtracted.

precipitates are still connected to one another but now form strings homogeneously distributed in the magnesium matrix. Such an organization induces strain fields in the matrix in the neighbourhood of precipitates (Fig. 8), and also promotes a long dimension in the precipitated phase. Volume fraction of precipitates is larger than in the T6 state; the small dimensions are slightly larger, but there is now a long dimension (Antion *et al.*, 2007, in preparation).

Corresponding SAXS measurements show that intensity is not qualitatively different between the T6 and T8 states, probably because the influence of the length of strings is at too small q values. Streaks are stronger as seen in Fig. 9. At large q , intensity also exhibits a q^{-4} behaviour. A Kratky plot (Iq^2 vs q) on Fig. 10 shows a maximum of Iq^2 , which should be related to a gyration radius (Deschamps *et al.*, 2003). But this maximum is very close to the beam-stop and is not really reliable. Because integrated intensity is the integral of this curve, it is highly probable that a part of it is not measured.

4. In-situ measurements

Evolution of mechanical properties with temperature of both quaternary alloys in their T8 state has been tested using compression tests (Table 2). The compression tests begin as soon as temperature is reached (with a heating rate of 0.5°s^{-1}); the yield point is reached within 40 to 50 s. In order to correlate mechanical behaviour with evolution of hardening precipitation, SAXS measurements have been carried out during *in situ* thermal annealing of samples previously in the T8 state. Experiments have been made at 523 K, 548 K and 573 K, with the same heating rate of 0.5°s^{-1} .

Integrated intensity = $\int I(q)q^2dq$ is probably truncated in the small q -range, so we will call it

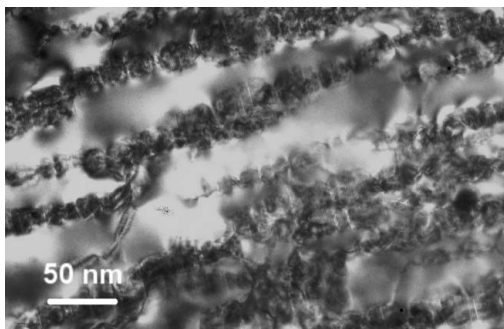


Figure 8
Bright field images of 4Gd-5Y in T8 state showing strings of connected β' precipitates, and the associated strain field.

'partial integrated intensity'; to evaluate the large q contribution, $I(q)$ has been fitted to $Aq^{-4} + B$ in the q -range ($0.08\text{--}0.13 \text{ \AA}^{-1}$), B has been subtracted, and the analytical extrapolation has been added. With the *in-situ* measurements being done at a fixed place in the sample, comparisons are justifiable.

The time origin was chosen as the time 473 K was reached. These annealing treatments induce an immediate decrease of partial integrated intensity, in agreement with lower volume fraction f_v of the β' precipitates (Fig. 11). This decrease is too fast to be attributed to coarsening (Nicolas & Deschamps, 2003). After several minutes, intensity stabilizes, or increases slowly.

At 523 K, the decrease of intensity is small, and the shape of the intensity curve does not change too much. This means that β' precipitates remain stable at 523 K, with only a small decrease of f_v . The yield stress value is measured too early to be influenced by the f_v decrease.

At 548 K, the decrease of intensity is much more important and the decrease is rapid enough in order to part account for the loss of mechanical properties reported here.

At 573 K, the decrease of intensity is greater and nearly completed during heating; the compression tests being performed after f_v decreases, the strong decrease of yield stress is representative of the low volume fraction of β' . Some time later, a new phase nucleates, increasing $I(q)$. The nucleation of a new phase, favoured by the release of solute due to β' dissolution, is consistent with the calculations of phase diagrams in the Mg-Mn-Y-Gd (Antion, 2003) system, which predict the appearance of equilibrium β phase in this range of temperature for both alloys.

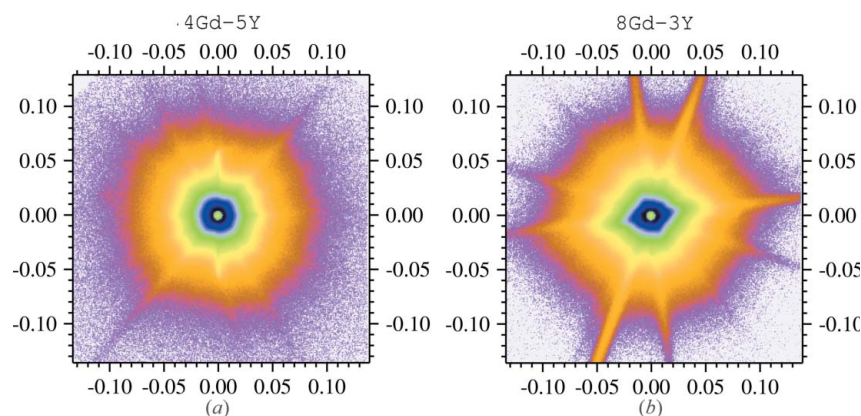


Figure 9
Two-dimensional rough intensity maps for 4Gd-5Y and 8Gd-3Y in T8 state (unit on the axes are \AA^{-1} , auto-scaled intensity).

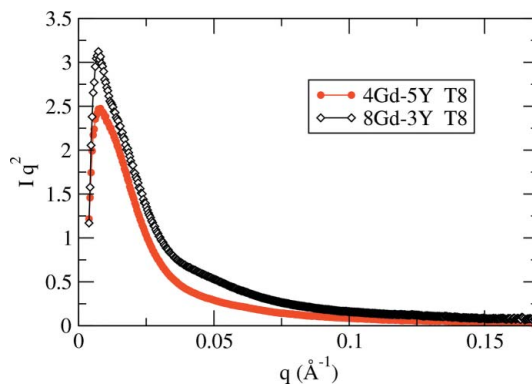


Figure 10
Kratky plot (Iq^2 vs q) for both 4Gd-5Y and 8Gd-3Y alloys in T8 state.

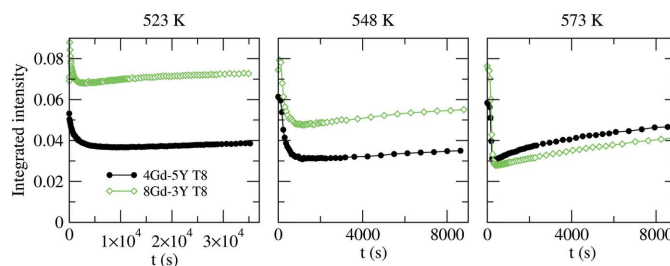


Figure 11
Partial integrated intensity for different annealing times at the indicated temperature.

5. Conclusions

We have demonstrated the presence of GP zones in the quaternary Mg-Gd-Y-Mn alloys in the T4 state, which are absent in the binary Mg-Y alloy. GP zones may be helped by the presence of gadolinium in quaternary alloys. They were also detected in commercial WE43 (Mg-Y-Nd) alloys in a previous study.

Using anomalous scattering at the Y edge we have shown that the precipitates of the equilibrium β phase have a different chemical composition in the 8Gd-3Y' alloy (mainly Gd-rich) as compared with the 4Gd-5Y alloy (mainly Y rich), in agreement with their difference in crystallographic structure. In addition, it has been shown that the metastable β' phase has a different composition in Y as compared with the equilibrium β phase.

In the T6 and T8 precipitation hardened states the scattering is strongly influenced by the phase morphology. Different shapes of streaks present in the two-dimensional scattering images have been related to the microstructures observed by HRTEM.

The evolution of the microstructure in the T8 state subjected to a heat treatment in the temperature range 523–573 K has been followed by *in-situ* SAXS measurements. Partial dissolution of the metastable β' phase has been observed at short ageing times, followed by re-precipitation of a new phase for the highest temperature. This partial dissolution has been shown to be consistent with mechanical properties measured early on in the same temperature range. A mechanical test after longer annealing times must be performed to have a better knowledge of performances with temperature of these alloys.

We are grateful to the ERSF, Grenoble, for access to the French CRG beamline D2AM and the help of its technical staff, J.-F. Berar, N. Boudet, B. Caillot and S. Arnaud.

References

- Adachi, H., Isogai, J. & Osamura, K. (2004). *Trans. Mater. Res. Soc. Jpn*, **29**, 97–100.
- Antion, C. (2003). PhD thesis, INPG, Grenoble, France.
- Antion, C., Donnadiou, P., Perrard, F., Deschamps, A., Tassin, C. & Pisch, A. (2003). *Acta Mater.* **51**, 5335–5348.
- Antion, C., Donnadiou, P., Tassin, C. & Pisch, A. (2006). *Philos. Mag.* **86**, 2797–2810.
- Antion, C., Donnadiou, P., Tassin, C. & Pisch, A. (2007). In preparation.
- Anyanwu, I. A., Kamado, S. & Kojima, Y. (2001). *Mater. Trans.* **42**, 1206–1211.
- Deschamps, A., Bley, F., Livet, F., Fabregue, D. & David, L. (2003). *Philos. Mag.* **83**, 677–692.
- Goerigk, G., Haubold, H.-G., Lyon, O. & Simon, J.-P. (2003). *J. Appl. Cryst.* **36**, 425–429.
- Guinier, A. & Fournet, G. (1955). *Small-Angle Scattering of X-rays*. New York: Wiley.
- Nicolas, M. & Deschamps, A. (2003). *Acta Mater.* **51**, 6077–6094.
- Nie, J. F. & Muddle, B. C. (1999). *Scr. Mater.* **40**, 1089–1094.
- Nie, J. F. & Muddle, B. C. (2000). *Acta Mater.* **48**, 1691–1703.
- Porod, G. (1982). *Small Angle X-ray Scattering*, edited by O. Glatter & O. Kratky. London: Academic Press Inc.
- Simon, J. P., Arnaud, S., Bley, F., Berar, J. F., Caillot, B., Comparat, V., Geissler, E., deGeyer, A., Jeantey, P., Livet, F. & Okuda, H. (1997). *J. Appl. Cryst.* **30**, 900–904.
- Simon, J. P. & Lyon, O. (1987). *Philos. Mag. Lett.* **55**, 75–80.
- Tchoubar, D. & Mering, J. (1969). *J. Appl. Cryst.* **2**, 128–138.